CHALMERS
UNIVERSITY OF TECHNOLOGY

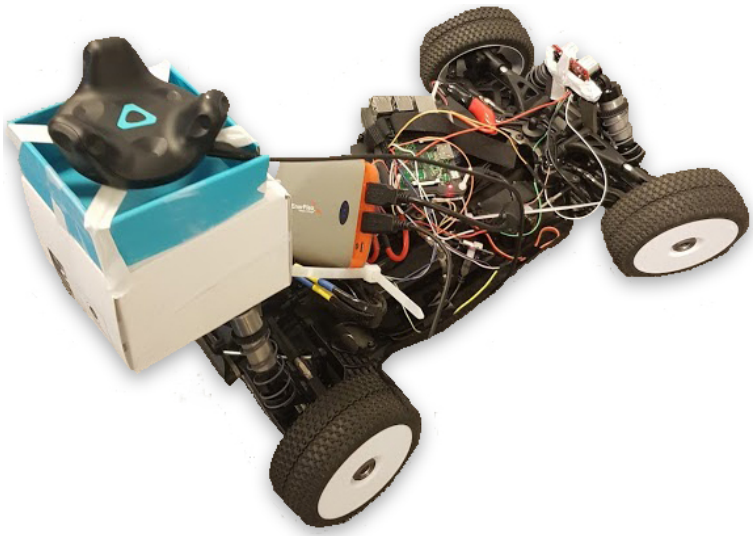

Generic Sensor Error Modelling

Using Radar Equation for Estimating the Sensor Error in Ultrasonic Sensors

Master's thesis in Biomedical Engineering and Complex Adaptive Systems

PER OLZON and VANESSA VANNAS

Department of Electrical Engineering
CHALMERS UNIVERSITY OF TECHNOLOGY
Gothenburg, Sweden 2020

Master's thesis 2020

Generic Sensor Error Modelling

Using Radar Equation to Estimate the Sensor Error in Ultrasonic Sensors

PER OLZON AND VANESSA VANNAS

CHALMERS
UNIVERSITY OF TECHNOLOGY

Department of Electrical Engineering
Chalmers University of Technology
Gothenburg, Sweden 2020

Generic Sensor Error Modelling
Using Radar Equation to Estimate the Sensor Error in Ultrasonic Sensors
PER OLZON and VANESSA VANNAS

Supervisor: Ole Martin Christensen, Qamcom Research and Technology
Supervisor: Shen Li, Department of Electrical Engineering, Chalmers University of Technology Examiner: Fredrik Brännström, Department of Electrical Engineering, Chalmers University of Technology

Master's Thesis 2020 Department of Electrical Engineering
Chalmers University of Technology
SE-412 96 Gothenburg
Telephone +46 31 772 1000

Cover: The vehicle used in the thesis, which is controlled by a Raspberry Pi.

Typeset in LaTeX
Gothenburg, Sweden 2020

Generic Sensor Error Modelling
Using Radar Equation and Sensor Fusion to estimate the Sensor Error in Ultrasonic Sensors
PER OLZON and VANESSA VANNAS
Department of Electrical Engineering
Chalmers University of Technology

Abstract

Participating in everyday activities is difficult for disabled individuals that are unable to drive their electric wheelchair on their own. They have to rely on a third person to orientate in public areas. A solution to the problem might be an autonomous powered wheelchair. This wheelchair needs to be able to navigate in mapped and unknown areas without hitting obstacles and therefore relies on information from different kinds of sensors mounted on the vehicle. These sensors need to be as precise as possible, not to provide the wrong information to their user.

The goal of this project is to investigate the failure rate in ultrasonic sensors and if it is possible, using radar equations, to generate a generic model to predict the failure rate and in turn avoiding it. The setup contains two ultrasonic range sensors (HC-SR04 and JSN-SR04T), one Raspberry Pi 3, a HTC VIVE system and a radio-driven car. Using the HTC VIVE system as a reference system is tested separately. The sensors are then mounted on the radio-driven vehicle and tested with the HTC VIVE system both in stand-still and in motion. The data is analyzed using a Savitzky-Golay filter to detect and smooth out the outliers.

Results from the sensor experiments indicates that the HC-SR04 sensor is worse than the JSN-SR04T sensor at detecting objects, but the JSN-SR04T sensor sometimes detects unwanted objects. When running vehicle experiments, the JSN-SR04T sensors failure rate is therefore much larger than for the HC-SR04 sensor. The standard deviation for the sensors was not of the same magnitude as the standard deviation for the stopping distances of the vehicle. This indicates that, not only the sensor errors should be considered when designing an emergency braking system, but also the delays in the system can be as important. The results from the vehicle experiments shows that the HTC VIVE system is not suitable for real-life applications, but can have enough accuracy for test environments. When using the HTC VIVE system more than one tracker needs to be used, since the reference system in the HTC VIVE system has a tendency to drift.

Using ultrasonic sensors for detecting obstacles at medical autonomous vehicles are possible in experimental environment but more research in the area are necessary to ensure safety for the users in real life environment.

Keywords: sensor failure, generic model, ultrasonic sensors, radar equation, autonomic powered vehicle.

Acknowledgements

We would first like to thank and acknowledge the work and dedication that our thesis supervisor Ole Martin Christensen at Qamcom has put into guiding us forward during the process. We furthermore like to thank the rest of our colleagues at Qamcom for providing an open and stimulating working environment, and especially Carl Bergenhem, Andreas Johansson, Carl-Michael Wagner and Johannes Wiig for their assistance and instructions on the VIVE system, vehicle construction and for participating in our practice presentation at Qamcom. This work is supported by VINNOVA via the FFI ESPLANADE project, see http://esplanade-project.se/. We also like to thank Fredrik Malmsten at Qamcom for answering our questions regarding the electronics laboration rooms and equipment. Further, we would like to acknowledge our second supervisor Shen Li and our examinator Fredrik Brännström from the Chalmers University of Technology. We are grateful for her valuable comments on the thesis.

Finally, we must express gratitude to our parents and friends for the unfailing support and encouragement throughout our years of studying at the Chalmers University of Technology and through the process of researching, testing and writing the thesis. This would not have been possible without them. Thank you.

Per Olzon and Vanessa Vannas, Gothenburg, February 2020

Abbreviations

Echo level (E_L)
Enhanced Time to Collision (ETTC)
Event Tree Analysis (ETA)
Failure Mode and Effect Analysis (FMEA)
Fault Tree Analysis (FTA)
Field of View (FoV)
General-Purpose Input/Output) (GPIO)
Ground (GND)
Pulse Width modulation (PWM) Savitzky-Golay filter (GS-filter)
Source level (S_L)
Target strength (T_S)
The National Highway Traffic Safety Administration (NHTSA)
The Raspberry pi 3 Model B (RPI3)
The Ultrasonic Ranging Sensor (HC-SR04)
Time to Collision (TTC)
Transmission Control Protocol (TCP)
Transmission loss (T_L)
United Nations (UN) Voltage Common Collector (VCC)
Waterproof Ultrasonic Distance Arduino Sensor (JSN-SR04T)

Contents

List of Figures

List of Tables

1

Introduction

Studies on autonomous vehicles have been a discussed subject in both science and media. A significant point for autonomous vehicles is that they may reduce a portion of the fatal vehicle accidents caused by human errors [1]. During recent years there have been incidents involving autonomous vehicles, which have caused many countries to restrict the usage and testing for autonomous vehicles [1]. There are numerous explanations why the incidents happened, although sensor errors can be a contributing factor. The sensors used on vehicles to make them autonomous are not only adaptive at regular vehicles but may also be used in the biomedical field on for example powered wheelchairs. Sensor errors are as important in this field as in the field of autonomous vehicles. When designing an autonomous system, one important aspect is to calculate the sensor failure rate for all the sensors in the system. This process consumes much time due to its importance to safety in autonomous systems [2]. A total autonomous vehicle refers to a vehicle that is operated by a computer/robot and hence works without a human operator [3]. The computer controls the control functions (steering, throttle, braking and so on) without the interference of the driver [2].

There are several classification systems for automotive vehicles, for example, SAE standard and NHTSA standard that has five levels of automotive, from no automation to fully automation [1]. There are however few regulations or laws for powered accommodations. Some European Standards regarding medical devices are important in the work with powered wheelchairs [4] where especially EN ISO 14971:2012 [5] regarding risk management and EN 62304:2006 [6] regarding software life-cycle processes are used in several projects regarding biomedical aspects and sensors in Europe. More European Standards regarding medical devices and electrically powered wheelchairs can be found in Appendix A.2.

Individuals with visual, motor and/or cognitive disabilities may have difficulties maneuvering a powered wheelchair. Their disabilities might interact with their ability to maneuver the vehicle through doors, in small areas, for example in/out of elevator, at workspaces and so on in a safe, risk-free way for both the individual in the wheelchair and other individuals in the same area [7–11]. Their lack of maneuvering may be a hazard for the individual and their surroundings but is foremost time consuming and frustrating causing a more restricted everyday life. For individuals with disabilities, maneuvering the wheelchair in another way than with a regular joystick is an important aspect to gain independence and control of their daily life

[12]. The United Nations (UN) Convention on the Rights of persons with disabilities states that a person with a disability should be able to live as independently as possible and be able to participate fully in their life. This includes, for example, the physical environment and transportation [13]. The UN sustainability development goals [14] have 17 goals that should be focused on to sustain and promote a new worldview. A generic model for sensor failure might be a step towards a more accessible environment for a disabled individual affecting the goals in Health and population dynamics, sustainable cities and settlements and employment and decent work for all. The individual can be more independent and be able to participate in more activities in a difficult physical environment, apartments, work areas, hospitals and so on with less safety risk [13].

High reliability in a vehicle is important since the failure of the components or the sensors on the vehicle (both cars and powered wheelchairs) may cause serious accidents [15]. Important aspects are that the system needs to be able to handle bad weather conditions, environmental hazards, equipment failures, traffic rule violations from other vehicles, animals and children on the road and expected and unexpected obstacles [16]. Trust in an autonomous vehicle means to trust in the technology of the vehicle to fulfill the task of traveling safety and without accidents from point A to point B. Some fears that occur at present time are that the vehicle may have problems due to failures in the equipment and due to environmental impacts causing safety issues for the vehicle itself with an accident as a result [17]. This shows the importance of sensors with robust failure analysis applied to them, to mitigate problems with the sensors [18]. The reliability and the levels of autonomy of the system are important factors for the users with disabilities when it comes to technical aids or the navigation system of a powered wheelchair. The system does not need to be completely autonomous since the user wants to complete the task as much on its own as possible [19]. Hence the system can be semi-autonomous and only correct/take over from the driver when an obstacle is in the way for the wheelchair [7].

In this thesis, we aim to develop and implement a generic model for sensor failure with a focus on range sensors. The work is motivated by the need to understand how to mitigate the failure rates for an autonomous vehicle system. The sensors can be tested on a powered wheelchair to ease individuals unable to drive the vehicle by themselves to access and participate in activities in a public environment. The purpose of these experiments is to estimate the error from the sensors and how it varies depending on the distance from the object and if several sensors are used. The results from the experiments should then be used to find a generic model for the sensor error. The project was implemented in several parts. Firstly a literature review was carried out with the purpose to precise the goals for the project, collect information for the final report and extend our knowledge about the subject and find the state of the art on Sensor Failure Modelling according to the generic model [20]. The next step was to identify the requirements of the failure model and implementing a generic sensor failure model. This contained a sensor experiment, designing the system and vehicle experiment to develop a generic method for sensor failure in autonomous vehicles.

2

Background

A sensor is an electronic device used to detect signals or changes from its surrounding and returning the detected signals for analyzing by, for example, a computer. There is a wide range of different sensors at the market, used in our daily life and in different areas, for example in a vehicle, in the field of medicine and robotics. A sensor needs to be sensitive to the subject it is used to detect and insensitive for other subjects in the same area [21].

Speed sensors, for example, LiDAR and Radar are used to detect the velocity of an object but can be affected by the surrounding environment. Radar sensors use an electromagnetic wave instead of sound waves to measure the distance between the sensor and the target object. The function of the radar sensor is similar to the ultrasonic sensor but it has a faster speed of the waves. The radar sensor is less affected by temperature, weather conditions and uneven surfaces than the ultrasonic sensor and has higher accuracy. The target surface must, however, have enough dielectric constant to reflect the electromagnetic wave otherwise the signal misses the object [21].

Ultrasonic distance or range sensors are used to measure the distance between the sensor and the target object using ultrasonic, acoustic waves. The sensor can be used in several areas, for example, to measure the liquid level in tanks or monitor sea levels. It can also be used in the field of autonomic vehicles and unmanned aerial vehicles to detect objects and obstacles that may hinder the vehicles. The ultrasonic sensor can create a safe path with correct accuracy and reliability for the vehicle and hence avoid crashes and accidents with other vehicles or objects [22, 23]. The sensor is efficient in for example bad weather conditions and on areas with good reflections but the signals can be absorbed by the material and can hence be reflected to a wrong way causing an error in the measurement. A stronger signal might be needed from the sensor if the target surface is soft or uneven [23, 24].

Some advantages of using an ultrasonic sensor are that the ultrasonic sensor is a cheaper option than other sensors and the appearance of the target object, for example light, dark or transparent color, does not affect the measurement. The ultrasonic sensor can also be used in difficult weather conditions and environments, for example sunny/dark, dusty or foggy weather conditions [24–26]. However, the ultrasonic sensor has some disadvantages. At the moment the range of the ultrasonic sensor is about 20 m which is shorter than the range of the long-range LiDAR sensors and radar sensors that can operate on distances of 250 m [27].

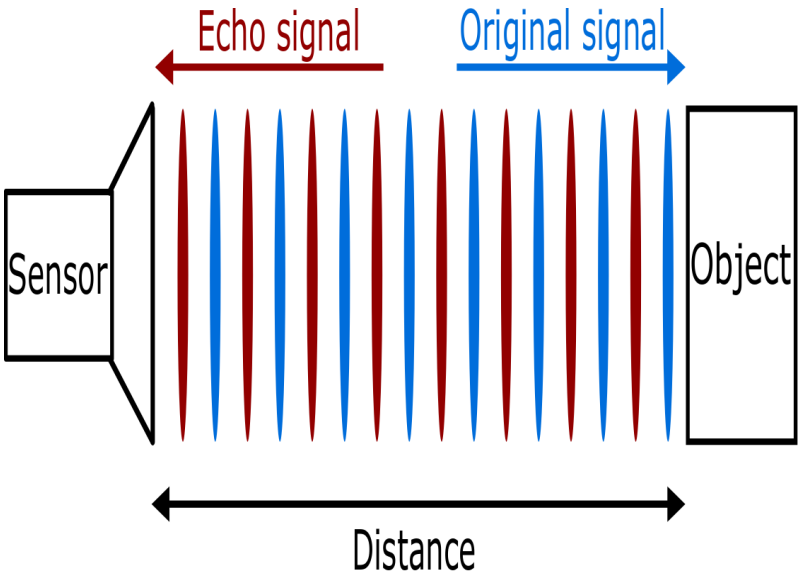

Figure 2.1: The function of an ultrasonic sensor. The transducer in the sensor provides the original signal (acoustic wave), the wave then reflects with the object causing a reflected wave in the opposite direction described as the echo signal. The echo signal then returns to the receiver in the sensor. The time it takes for the signal to travel from the object to the receiver is used to provide the distance from the object to the senor using Equation 3.9.

The signal of the ultrasonic sensor can be affected by the material context of the object and may vary if the surface of the object contains soft fabric or is a concrete wall. The resulting signal from the ultrasonic sensor also varies based on the context of the surface and the sensor can not measure at high repetition rates without interfering with itself [26]. The ultrasonic sensors can mostly manage difficult weather conditions and environments due to that the signal from the sensor is a sound wave (echo). The sound wave can detect the object more efficiently than for example a light wave. A sensor using a light wave can be affected by object appearance or weather conditions by deflecting or absorbing the wave, resulting in false readings [21]. The transducer in the ultrasonic sensor sends out a wave, that hits the object and echoes back to the receiver where the emitted waves travel with the speed of sound [21, 22]. The time it takes for the echo signal to return to the receiver is called receiver time and is used to detect how far away the object is located [22]. An illustration of how the ultrasonic sensor is operating can be seen in Figure 2.1 [24]. In this thesis, ultrasonic sensors are used in the experiments.

2.1 Sensor Parameters

The reflection coefficient is described in the literature as the back-scattering coefficient. The back-scattering coefficient σ_0 is dimensionless and depend on the incidence angle θ, and possibly also on the corresponding azimuth angle ϕ. Values of σ_0 are a result of a scattering matrix depending on the Stoke vector for radiation

[28]. Not knowing the phase of the reflection coefficient from the sensor is called a mismatch uncertainty. The uncertainty takes into consideration the amount of power which usually is measured in dB m, that is unavailable at the output created by signal reflection and impedance mismatches. The uncertainty can be reduced by optimizing the reflection coefficient for example by minimizing the length of the cables used in the setup, by reducing the numbers of adaptors or using the same type of connector throughout the entire setup. A calibration factor, K_b, reveals the uncertainty inefficiency of each sensor, mismatch loss, and reflected signal [29]. The accuracy of the sensors can be affected by several factors. The sensors have a limited range for the output signal and therefore do not work outside this range. Another factor can be a sensitivity error where the measured signal may differ from the actual value, the sensor can be disturbed by noise and may be influenced by the surrounding environment.

Noise is a factor that affects the measurements of all kinds of sensors. The presence of noise creates variations in the results, making it different from reality. There are different types of noises that can be generated from models based on sensor errors. The quantization noise occurs when the analog signal is discretized when measured. The random walk noise is present in many real-world processes, such as stock markets, diffusion, and gyroscopic measurements. If the random process is slower, the noise is called bias instability or flicker noise. The noise presents itself as a slow drift in the measurements over a larger time. Rate ramp noise has a low-frequency drift in the sensor noise presented as a deterministic error of long but finite time interval [30].

2.2 The State of the Art on Sensor Failure Modelling

Both internal and external sensors are affected by sensor failures which in turn affect the safety in the systems (application/actuators) and the safety for the users. According to Koopman and Wagner, the sensors are only able to predict a probability that an obstacle is present, but never provide a 100 % certainty [16]. Sensors that can adapt to the environment on the road are necessary for autonomously driven vehicles [20]. The sensors need to provide both spatial information (observations) and error characteristics. However, to be able to analyze a generic model, the sensor error characteristics are needed. Sensors transform non-electrical signals into electrical signals and can together with a computer algorithm identify obstacles in the surrounding environment. All sensors are prone to have errors or failures that can lead to the computer algorithm failing to identify the necessary objects. Different sensors have different parameters that need to be tuned to minimize errors. A generic model to detect sensor failure might be used for this purpose.

Jäger *et al.* describes three important areas for a generic model: *Identifying requirements on failure models*, *State of the Art on Sensor Failure Modelling* and *Introducing a Generic Sensor Failure Model* [20]. An appropriate failure model is according to the author required to have a generic approach to the characteristic of the failure and it must be able to represent different failures. The means in the failure model must be unique and allow analysis on different levels. A failure model that fulfills these requirements are needed.

Jäger *et al.* describes three different approaches to a statically composed system: FMEA [31], FTA [32] and ETA [33]. These methods are used to influence failure models that take the components error characteristics and fault tolerance into account during the design of the system to minimize the effect from the error and hence limit component failure and increase the safety level. The design of the system does not change during run-time. A dynamic composed system has an integration step that can use the information from the environment in different but cooperative processes, resulting in increased autonomy, increased range and decreased demands on the local sensors. The dynamic system lacks information in failure characteristics from the external sensors in the design phase, which results in a need for deeper understanding during the sensor selection and system design. The design of the system is more dependent on the information from the sensor errors during run-time.

3

Methods

In this chapter, the theory of the radar range equation will be presented. After that, the test and evaluation procedures are described. Finally, approaches to identifying the outliers, hence sensor failures, presented in the data will be covered.

3.1 Radar Range Equations

The radar range equations are used to describe environmental factors, system specifications and properties that affect measurements from ultrasonic sensors and radar sensors. The equation is used to detect the amount of the signal that is returned to the sensors and the amount of noise that disturbs the signal [34]. A modified radar equation from a sonar equation: $E_L = S_L - 2T_L + T_S$, can be used on measurements from the ultrasonic sensor, since the operation on both sensors are similar to each other. For both ultrasonic and radar sensors, the receiver and the transmitter are monostatic, hence having the same gain (G). The echo level (E_L) spread in the same way and depends on the amount of power that is echoed to the receiver [35]. The E_L is based on the strength of a signal returning to the sensor after hitting an object. The equation consists of a source-level (S_L) for the signal corresponding to the signal strength from the sensor, a transmission loss (T_L) for the signal corresponding to the loss of signal strength in the area between the target and the sensor and a target strength (T_S) corresponding to the amount of the signal strength returning from the target. The T_L is multiplied by two due to that the signal has to travel to the target and back to the sensor, hence two ways. In our study, there are no measurements of the S_L, only the sensor information in Table A.1. The sonar equation is based on a logarithmic scale and therefore harder to apply to our project. The equation, therefore, needs to be rewritten into the radar equation.

$$I_{\text{inc}} \cdot \sigma = I_{\text{refl}} \cdot 4\pi R^2 \rightarrow \frac{I_{\text{refl}}}{I_{\text{inc}}} = \frac{\sigma}{4\pi R^2} \tag{3.1}$$

The reflected power from a sensor can be described as Equation 3.1. With these measurements, the approximate threshold for the sensor can be estimated. The ratio between the incident power, I_{inc}, to the reflected power, I_{refl}, can be seen in Equation 3.1, where σ is the cross-section of the object, and R is the distance from the source. The reflected signal will be absorbed by the sensor, which has the width

of the sensor (σ_{sensor}). The same expression as Equation 3.1 can be used, by changing I_{refl} to absorption.

$$\begin{aligned} \text{In dB: } T_L &= 20 \cdot log(R) + R\alpha \\ \text{In comparison to input: } T_L &= R^2 + 10^{\alpha R} \end{aligned} \tag{3.2}$$

The T_L can be seen in Equation 3.2. In the second term, α is the absorption coefficient. Since the measurements have been in the air, this absorption coefficient can be set to zero [34].

$$E_{L\text{intensity}} = I \cdot \frac{1}{(2R)^2} \cdot \frac{\sigma}{4\pi R^2} \cdot \sigma_{\text{sensor}} = \frac{\sigma}{16\pi R^4} \cdot I \cdot \sigma_{\text{sensor}} \tag{3.3}$$

$$E_{L\text{intensity, wall}} = \frac{\Omega}{16\pi R^2} \cdot I \cdot \sigma_{\text{sensor}} \tag{3.4}$$

The E_L, with regards to the intensity for the sensor, can be seen in Equation 3.3. With this model, the threshold for the sensor can be estimated. If the measurement is against a flat surface, for example, a wall, the equation is simplified as in Equation 3.4. The Ω in the equation is the solid angle, defined as $\Omega = \frac{\sigma}{R^2}$. The equation is similar to the radar range equation described below in Equation 3.5 to Equation 3.8.

$$P_{di} = \frac{P_t}{4\pi R^2} \tag{3.5}$$

$$P_{de} = \frac{P_t G}{4\pi R^2} \cdot \frac{\sigma}{4\pi R^2} \tag{3.6}$$

The power density, P_{di}, of a radar, applied for isotropic antennas, where P_t is the amount of the transmitted power, is viewed in Equation 3.5. If the antenna is directional, G is added to Equation 3.5, which shows how power decreases according to the length. The reflected power, P_{de}, is viewed in Equation 3.6 [36].

The power that is received by the radar, P_r, is affected by the aperture (opening), A_e, of the receiving antenna. The received power then becomes:

$$P_r = P_{de} A_e = \frac{P_t G}{4\pi R^2} \cdot \frac{\sigma}{4\pi R^2} A_e \tag{3.7}$$

By solving this equation for R, the maximum range for that radar can be found. The equation is dependent on the size of the target [36].

Sensor	Max Range [cm]	Min Range [cm]	FoV [cm]	Accuracy [cm]
JSN-SR04T	600	20	75°	±1
HC-SR04	400	2	15°	±0.3

Table 3.1: The max range, the min range, the FoV and the accuracy from the datasheets of the JSN-SR04T and the HC-SR04 sensors.

$$
\begin{aligned}
P_r = P_{de}A_e &= \frac{P_tG}{4\pi R^2} \cdot \frac{\sigma}{4\pi R^2}A_e \\
\Rightarrow P_r &= \frac{P_tG\sigma A_e}{(4\pi)^2R^4} \\
\Rightarrow R^4 &= \frac{P_tG\sigma A_e}{(4\pi)^2P_r} \\
\Rightarrow R &= \left[\frac{P_tG\sigma A_e}{(4\pi)^2P_r)}\right]^{1/4} \\
\Rightarrow R_{\max} &= \left[\frac{P_tG\sigma A_e}{(4\pi)^2S_{\min}}\right]^{1/4}
\end{aligned}
\tag{3.8}
$$

In the last step of Equation 3.8, P_r is replaced by $S_{\min}$ which is the minimal signal the system can detect, making the equation the way it is usually expressed [36].

3.2 Test and Evaluation Procedures

The experiment setup contained two sensors, a breadboard, wires, resistances and a microcontroller (The Raspberry Pi 3 Model B (RPI3)). Two ultrasonic distance sensors, HC-SR04 [37] and JSN-SR04T [38] were used to estimate the distance between the transducer in the sensor and an foreign object.

The Ultrasonic Ranging Module HC-SR04-sensor contains an ultrasonic transmitter, a receiver and a control circuit. The sensor has four pins: the VCC (power 5 V), the Trig (trigger), the Echo (receiver) and the GND (ground). The pins Trig and Echo are connected to GPIO-pins on a RPI3, VCC are connected to the 3.3 V pin, illustrated in Figure 3.1 [37, 38]. The Arduino JSN-SR04T sensor is similar to HC-SR04 but differs in the fact that it has a 2.5 m long cable connecting the sensor and the breakout board, it is waterproof and has only one transducer. The transducer is therefore both a transmitter and a receiver. The sensor also has a higher max range than HC-SR04 and a field of view (FoV) at 75° compared to 15°. For more detail the reader is referred to Table A.1 in Appendix A.1 [37, 38]. The max range, the min range, the FoV and the accuracy for each of the sensors are presented in Table 3.1.

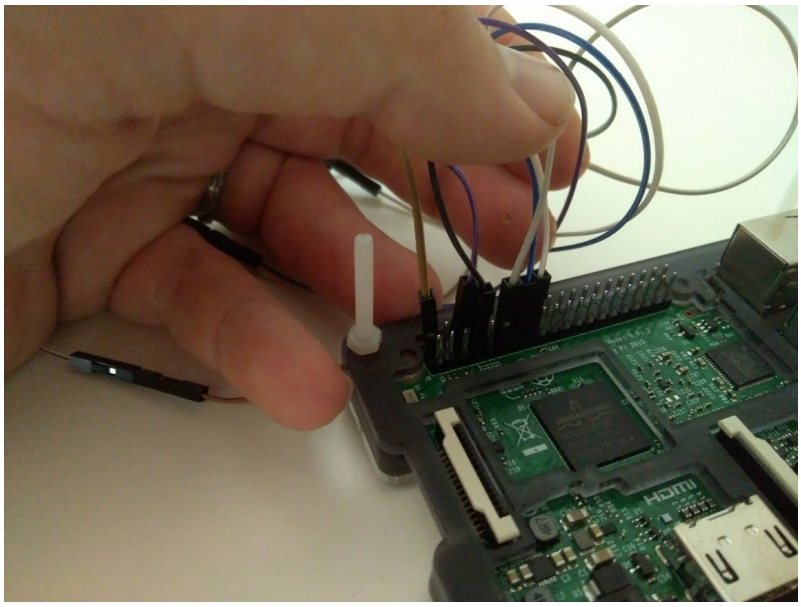

Figure 3.1: The figure shows the wires that connects the GPIO pins on the RPI3 to the pins on the sensors.

A microcontroller (RPI3) was used to communicate with the sensors, illustrated in Figure 3.1. Since the RPI3 is accepting 3.3 V as an input voltage, the output voltage from the sensors (5 V) needs to be dampened using a voltage divider [37]. To trigger the sensor to begin measuring, a short signal needs to be sent to the trigger pin. This signal needs to be at least 10 µs or more to cause the sensor to start a measurement. At the start of the measurement, the sensor generates acoustic waves and activates one of the output pins. These acoustic waves have a certain pattern and the sensor waits until this specific pattern returns as an echo. When the sensor detects the pattern, it will deactivate the output pin. By measuring how long the output pin was activated, the length to the target which the echo bounced against can be measured.

$$\text{distance} = \frac{\text{time} \cdot \text{speed of sound}}{2} \tag{3.9}$$

By applying Equation 3.9 the distance is found for the target object [39]. The time in Equation 3.9 is the time it takes for the wave to travel from the transmitter via the target object and back to the receiver. The speed of sound was set to $343\,\mathrm{m\,s^{-1}}$, but this is only true for a temperature of 20 °C and is fluctuating largely depending on temperature. Since the experiments were done in an office with close to constant temperature the fluctuations were not considered in this study.

3.2.1 Sensor Experiments

The first part of the project was to identify the requirements for failure models. This was done by measuring the signals from both sensors, separately when the signals were stand-still, mounted on a breadboard. This method was a statically composed system. The sensors were in the first test placed at a distance of 88 cm between the sensors and a plain, flat, white wall. In the second test, a drinking glass was placed between the sensors and the wall at a distance of 43 cm from the sensors. The distance of 43 cm was the possible smallest distance before the HC-SR04 sensor and the JSN-SR04T sensor failed with NaN as results. The distance of 88 cm was the furthest distance from the wall that the breadboard could be placed on the experiment table. The drinking glass had a diameter of 8.5 cm. The results from the measurements were analyzed with the purpose to create a sensor failure model. Figure 3.2 shows a simplified model of the setup when measuring failures in sensors.

The measurement series was run for at least 20 000 measurement points. The measurements intended to be able to parameterize the sensor failure which according to Equation 3.8 depends on the length from the sensor to the target object, L2-L1, and the cross-section for both the sensor, σ_1, and the target object, σ_2. A numerical solver that fits the peak of a normal distribution was used to receive the resulted graphs and tables presented in the result section. The mean deviation, standard deviation, and the failure rate are presented in the result for each data set in Chapter 4.

3.2.2 Designing the System

The sensor model was implemented and evaluated using data acquired with sensor HC-SR04 [37] and sensor JSN-SR04T [38] on a flat wall environment. The sensors were placed above each other on the frame of the vehicle and directed forward. Both the sensors were connected to the RPI3, and both triggered and collected the data from the sensors. This was done through the GPIO ports that are mounted on the RPI3. The output from the sensor can measure 5 V, while the GPIO ports on the RPI3 only can measure at 3.3 V. Therefore a step-down converter was made to step down the voltage from the sensor to the RPI3.

RPI3 was also connected to the motion control of the vehicle. By sending different frequencies pulse-width modulation (PWM), the sensor data were sent to another computer via Transmission Control Protocol (TCP) [40] to be processed. TCP was used since it provides ordered and error-checked deliveries, which results in a stream where none of the measurements are lost. The reason not to implement everything on the RPI3 was that the HTC Vive system was not compatible with the RPI3.

$$TTC = \frac{D_0}{V_r} \tag{3.10}$$

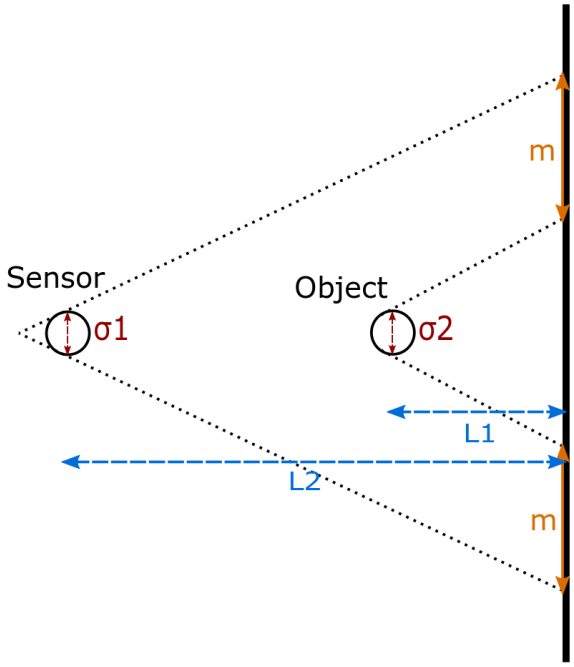

Figure 3.2: A simplified model of the second setup when measuring errors in sensors. During the first setup, the object was removed and the sensors were directly sensing the wall. σ_1 is the cross-section of the sensor and σ_2 is the cross-section of the target object. The variable $L1$ is the distance from the wall to the target object (drinking glass) and $L2$ is the distance from the wall to the sensor. The area m of the wall is the area that the sensor can detect, where the signals not reflected by the target object (drinking glass) are reflected. The signals reflected from the m-area takes longer time on returning to the sensor and can, therefore, be identified.

$$ETTC = \frac{-V_r - \sqrt{V_r^2 - 2 \cdot A_r \cdot D_0}}{A_r} \tag{3.11}$$

With the introduction of another computer and TCP, the delays of the system could no longer be assumed to be neglectingly small. Therefore predictions of the position of the vehicle needed to be implemented. A model was chosen as a predictor to calculate the speed according to the two latest measurements. By using this speed, the time to collision (TTC) was calculated from Equation 3.10 [41]. Enhanced time to collision (ETTC) is a better indicator of the braking process seen in Equation 3.11, but our measurements were not persistent enough to make good use of the ETTC. In Equation 3.10 an Equation 3.11 V_r is the relative speed/range rate between two vehicles, A_R is the relative acceleration between two vehicles and D_0 is the distance/range between two vehicles.

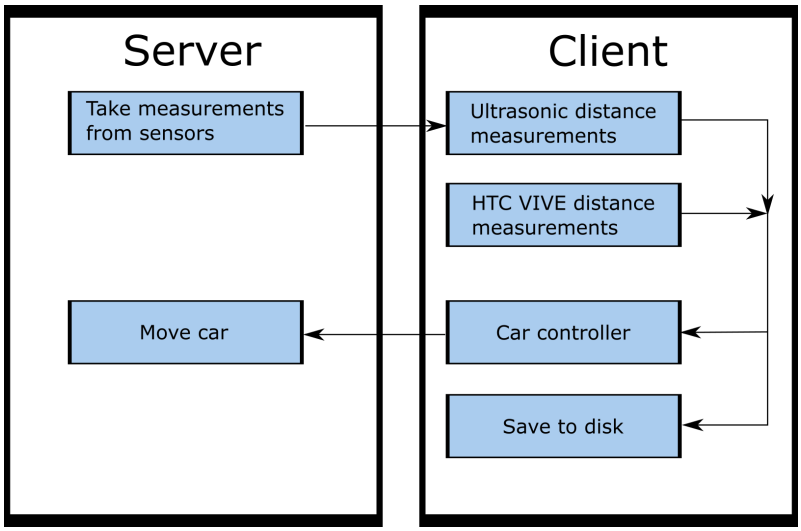

Figure 3.3: A schematic view of how the server (RPI3) and the client (computer) are transferring information. Results from the sensors are sent to the client with a timestamp. This provides the client with information that makes it possible to calculate the distance between the vehicle and the target object.

On the client computer, four different programs were run in parallel. The first program was calculating the distance according to the ultrasonic sensors. The second program was measuring the distance according to the HTC Vive system. The third program was sending commandos to the RPI3 to control the vehicle according to the distance. It also calculated the TTC to be able to stop the vehicle in time. The fourth program was saving all the data the other programs were generating and saved them to a hard drive, to be analyzed later.

Figure 3.3 shows how the different programs were interacting with each other. Notice that the client did all the calculations while the server was only sending measurements and responded according to how the client wanted to move the vehicle. This approach was implemented since the server had fewer resources than the client and since TCP already had to be implemented in the system, hence the faster client did all the calculations.

3.2.3 Vehicle Experiments

During the last part of the project, the autonomous vehicle was tested in a testing area at Qamcom, with the purpose to implement the generic sensor failure model designed from the results of the sensor experiment. The experiments were divided into several sub-experiments: the first for testing the HTC VIVE system, the second to test the sensors mounted on the vehicle from stand-still and the third to test the sensors in motion. During all the vehicle experiments both the JSN-SR04T sensor, the HC-SR04 sensor, and the HTC VIVE tracker were mounted on a radio-driven vehicle, according to Figure 3.4. The HC-SR04 sensor was mounted on top of the JSN-SR04T sensor probe. The RPI3 and a power bank can also be seen in Figure 3.4.

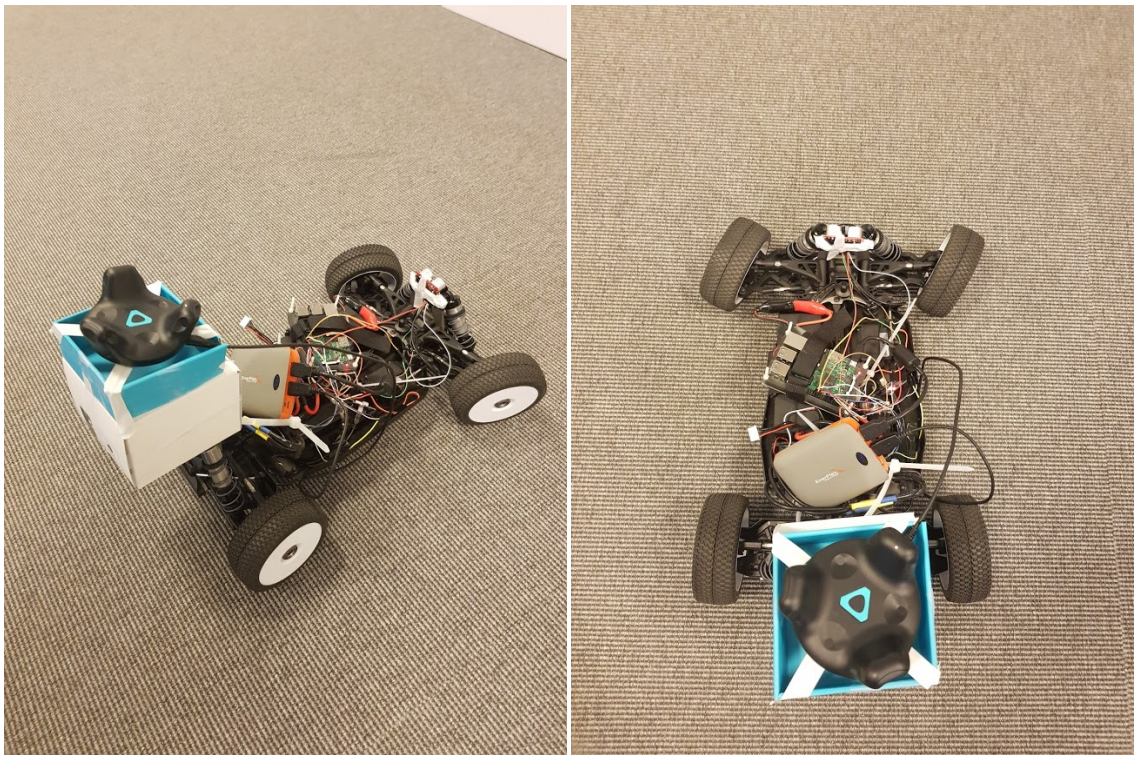

Figure 3.4: The radio drive vehicle used in the vehicle experiments. The location of the HTC VIVE tracker can be seen at the back of the vehicle and the sensors can be seen in the front of the vehicle. The HC-SR04 sensor is mounted over the JSN-SR04T sensor probe, not viable in the figure. The RPI3 and a power bank can also be seen in the figures.

3.2.3.1 Testing the HTC VIVE System

The HTC VIVE system is a virtual reality system developed by HTC. It contains base stationsthat communicated through infrared light (IR) with trackers called HTC trackers. The trackersconverts the signals from the base stations into Cartesian coordinates, which are transferred to and processed by a computer. The system can be controlled by hand controllers. This option was however overridden in this project. The HTC VIVE system is compatible with Steam VR and was used because it has enough API read measurements for the project. The HTC VIVE system in this project contained two base stations and three trackers. Two of them were used as a reference system and the last one was mounted onto the vehicle to track the motion of the vehicle.

The two trackers used as a reference system were mounted at the wall, and the height between the reference system and the tracker on the vehicle was calculated by the principle of the distance between a point and a line in space. By subtracting the height from the reference system, a two-dimensional system was obtained. The vector between the two trackers in the reference system was parallel to the wall.

Functions	Results
End-to-end latency	22 ms [42]
Accuracy (stationary)	<0.5 mm [43]
Accuracy (dynamic)	1 mm to 43 mm [43]

Table 3.2: The results from the literature study on the HTC VIVE system based regarding the end-to-end latency, stationary accuracy and dynamic accuracy.

By calculating the distance from the tracker on the vehicle to the vector, the distance from the wall was obtained. The end-to-end latency, stationary accuracy, and dynamic accuracy are presented in Table 3.2.

A problem with the HTC VIVE system is that the system does not have a solid reference system [44]. By changing the FoV of one of the base stations by a tiny amount, large changes in the coordinates given by the system were obtained. The system was also prone to drift if the vehicle was driven autonomously for more than two minutes. The three trackers were used to compensate for drift.

3.2.3.2 Static Measurements for the Vehicle

During this part of the experiment, the vehicle was positioned against a flat wall, with the sensors pointing against the wall. The vehicle was then reversed from the computer to stop 80 cm from the wall, as shown in Figure 3.5. This method was a dynamically composed system. The distance between the vehicle and the wall was measured by the HTC VIVE system and a ruler. If the ruler and the HTC VIVE system received the same values the first 20 times, then the rest of the measurements were taken only by the HTC VIVE system. The results aimed to achieve the error rate. This experiment was first performed using each sensor, separately (starting with the HC-SR04 sensor) and then using both sensors at the same time. The measurement series was run for at least 20 000 measuring points. The results were compared to each other to investigate if the generic model was working properly and if sensor fusion between the sensors had an effect on the returned signals, hence if the sensors interfered with each other.

3.2.3.3 Dynamic Measurements for the Vehicle

During this part of the experiment, the vehicle was positioned against a flat wall, with the sensors pointing against the wall, similar to the experiment before. The vehicle was then reversed to 150 cm and then driven back against the wall, to stop at a distance of 50 cm from the wall, see Figure 3.6. The distances between the vehicle and the wall were measured by the HTC VIVE system and the vehicle was driven by a computer. The results aimed to achieve the error rate. Since the sensor experiments showed that the sensors did not interfere with each other, this experiment was only performed with both sensors at the same time.

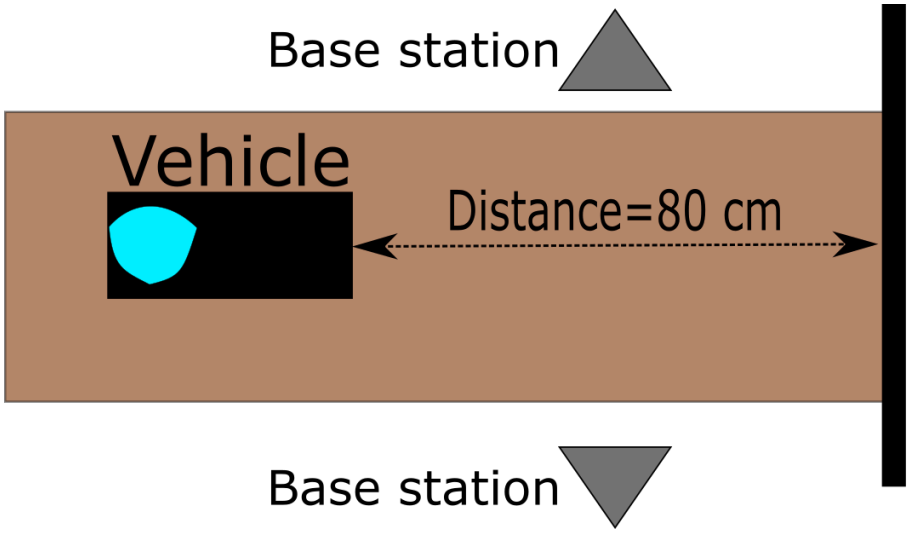

Figure 3.5: Experimental setup during stand-still experiments. The base stations are located on each side of the vehicle on half distance (75 cm) from the wall. The two trackers used as a reference system are mounted at the wall and the tracker used to track the vehicle motion is mounted at the vehicle. The starting position for the vehicle is against the wall, the first stop for the vehicle, after reversing, is at a target distance of 80 cm from the wall. The vehicle then returns to the starting point by driving into the wall. The experiment is conducted on a height of 75 cm.

The frequency of the sensors was not high, which forced to have a predictor of where the vehicle was positioned. This predictor was to measure the speed of the vehicle using the last two points. The vehicle was then assumed to drive at the same speed until a new measurement was obtained.

3.2.4 Analyzing the Data from the Vehicle Experiments and Identifying Outliers and Sensor Failure

There exist numerous of methods to decide outliers in time series [45]. Many of the methods for time series data are using regression to find outliers, where if the data is too far from regression it is classified as an outlier. The idea behind the implementation is that the vehicle is either moving forward or backward at almost constant speeds or is standing still. Therefore the measurements should form a smooth curve in the time domain. This is however not possible due to sensor failures causing outliers in the data. To receive the wanted, smooth result, a smoothing filter, Savitzky-Golay (SG) filter [46], is applied. The outliers are found by comparing the received raw data by the data processed by the SG filter. For a normal distribution, 95 % of the values are within two times of the standard deviation (2σ) of the mean value. The standard deviation on the raw data is analyzed compared with the smooth-filter, referenced as the mean value. All values that are above 2 m are directly removed before the identification of the outliers since they are visibly wrong. This method makes it possible to identify the outliers and process the sensor failure.

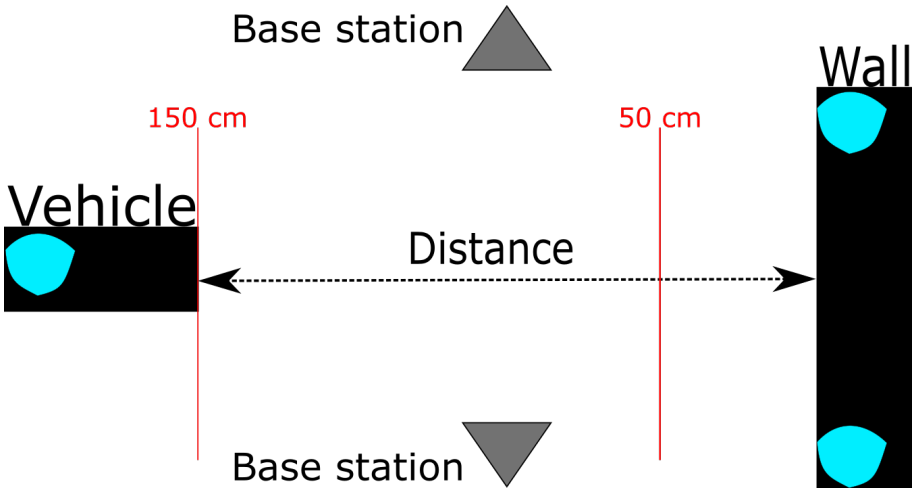

Figure 3.6: Experimental setup during motion experiments. The base stations are located on each side of the vehicle on half distance (75 cm) from the wall. The two trackers used as a reference system are mounted at the wall and the tracker used to track the vehicle motion is mounted at the vehicle. The starting position for the vehicle is against the wall, the first stop for the vehicle, after reversing, is at a target distance of 150 cm from the wall, the second stop for the vehicle, after forwarding, is at a target distance of 50 cm from the wall. The next starting point is at the second stop target distance of 50 cm from the wall. The experiment is conducted on the floor.

The SG filter is a convolution filter defined in the time domain, instead of the Fourier domain, which makes the transformation less computational heavy. The SG filter is showed in Equation 3.12, where m is the window size that corresponds to the number of nearest neighbours used in the linear combination, this gives $m = n_L + n_R + 1$. The SG filter replaces the data points with a convolution around each point. The variable n_L is the number of neighbours to the left/before a data point and n_R is the number of neighbours to the right/after a data point.

$$Y_j = \sum_{i=-n_L}^{n_R} c_i y_{j+i} \tag{3.12}$$

The simplest SG filter takes the average value over the nearest located points as its output, Yj, for example by setting $c_i = 1/m$ in Equation 3.12. This method is called moving average and is useful if the time series are changing linearly over time. Since sensor failures are not linear, a moving average filter cannot be used.

For nonlinear data, a higher polynomial approach can be used. Instead of setting the convolution coefficient c_i as a constant, the SG filter approximates the window size, m, to a quadratic polynomial. Each point in the quadratic window is then fitted with the least-squares estimation. The point i from the fitted polynomial is set as the value of Y_i. This process would be computationally heavy, but there are a specific set of convolution coefficients which accomplishes polynomial least-squared estimation fitting on a moving window using a linear design matrix.

The polynomial in Equation 3.13 of degree n is fitted at a point j in Equation 3.14 to receive c_i.

$$a_0 + a_1 j + \cdots + a_n j^n \tag{3.13}$$

$$y_{j-n_L}, \cdots, y_{j+n_R} \tag{3.14}$$

The design matrix for a polynomial least-square estimation fitting on a mowing window is viewed in Equation 3.15. Each row in the matrix is specific objects and each column is specific variables for each object. A design matrix is used as a general linear model to explain the correlation between the observed data and their variables 3.12.

$$A_{ij} = i^j, \quad i = -n_L, \cdots, n_R, \quad j = 0, \cdots, m \tag{3.15}$$

The normal equation for the vector of a_n in terms of y_j is viewed in Equation 3.16. This equation is used to receive the values from the polynomial based on j.

$$\mathbf{a} = (\mathbf{A}^T\mathbf{A})^{-1}(\mathbf{A}^T\mathbf{y}) \tag{3.16}$$

Since c_i is a_0 when y_j is a unit vector e_n, $-n_L < n_R$, the convolution coefficients become Equation 3.17. This shows that only one row in the inverse matrix is needed, and can be calculated by LU-decomposition using single back-substitution.

$$\mathbf{C} = (\mathbf{A}^T\mathbf{A})^{-1}\mathbf{A}^T \cdot e_n \tag{3.17}$$

4

Results

In this chapter, the results from the experiments are divided into two parts: identifying requirements on failure models through sensor experiments in front of a wall or a drinking glass as target object; introducing and testing the generic sensor failure model through vehicle experiments both in motion and at stand-still. The second part includes the results from the experiments where the vehicle in Section 3.2.3 were positioned in stand-still and motion. The results are discussed for the different parts.

4.1 Identifying Requirements on Failure Models Through Sensor Experiments

The first part of the project was to identify the requirements for failure models through a sensor experiment. This was conducted using both JSN-SR04T and HC-SR04 sensors, respectively, in two experiments, shown in Figure 3.2. The first sensor experiment was conducted against a wall at a distance of 88 cm from the sensor to the wall, measured by a ruler. The second sensor experiment was conducted with a drinking glass at a distance of 43 cm from the sensor to the glass, in front of the wall at a distance of 88 cm from the sensor. The measurement series was run for 50 000 measuring points for the distance of 88 cm and 20 000 measuring points for the distance of 43 cm. A numerical solver that fits the peak of a normal distribution was used, leading to the results in Table 4.1 and Table 4.2. The tables present the mean error, standard deviation and failure for each data set, distance, and sensor.

The measured distance is the distance measured with a ruler from the target to the front of the sensor. The minimum distance/range for both sensors can be found in Table 3.1. The distance of 88 cm was the furthest distance from the wall in these experiments. The mean error is the mean value of the difference between the distance measured with a ruler and the distance obtained from the sensor. The standard deviation is the standard deviation of the distance obtained from the sensor and the failure rate represents the measurements that are incorrect and not within the standard deviation ($2\,\sigma$) of the normal distribution over all measurements.

Sensor	True distance [cm]	Mean error [cm]	Standard deviation [cm]	Failure rate [%]
HC-SR04	5	-0.24	0.162	0.28
HC-SR04	25	0.99	1.03	0.02
HC-SR04	50	0.44	0.084	0.75
HC-SR04	88	0.49	0.09	0.09
JSN-SR04T	5	*	*	*
JSN-SR04T	25	-0.77	0.28	0.21
JSN-SR04T	50	-1.31	0.27	0.09
JSN-SR04T	88	-2.04	0.35	0.35

Table 4.1: The measured distance, the mean error, the standard deviation and the failure rate for the sensors for the first sensor experiment, with a wall as target object. The wall was located at a distance of 88 cm from the sensor. Only the largest peak is used in the table. The failure rate is all measurements that are not within the standard deviation, $2\,\sigma$, of the normal distribution. The symbol * represent distances for the JSN-SR04T sensor where a result is outside the range of the sensor. The minimum distance for the JSN-SR04T sensor is 20 cm, hence it is not possible to measure at 5 cm.

4.1.1 Sensor Experiment 1

The first sensor experiment, with a wall as target object, leads to the results in Table 4.1. Figure 4.1b and Figure 4.1a illustrate measurements against a wall at a distance of 88 cm for the JSN-SR04T sensor and the HC-SR04 sensor, respectively. The JSN-SR04T sensor has noise at 20 cm to 45 cm and at 70 cm to 81 cm. This indicates that the JSN-SR04T sensor detects more than just the target at longer distances. The HC-SR04 sensor has a peak located at 88 cm, where over 99 % of the measurements are located. A measured distance of 5 cm for the JSN-SR04T sensor is not tested since it is outside the sensors minimum range of 20 cm, presented in Table 3.1, and a result distance was not possible.

The mean error differs from -2.04 cm to -0.77 cm for the JSN-SR04T sensor and -0.24 cm to 0.99 cm for the HC-SR04 sensor. The JSN-SR04T sensor on average measures too short distances when compared to the true distance measured with a ruler. The HC-SR04 sensor, however, measure on average a distance that is larger than the true distance, which results in positive mean errors. An autonomic vehicle would in these cases hit the wall instead of stopping before. The measurements become less accurate for longer distances for the JSN-SR04T sensor, which is notably with higher standard deviations. This might be due to the sensor detects other objects than the target object because of its larger FoV at 75°.

The standard deviation for the HC-SR04 sensor varies from 0.08 cm to 1.03 cm, where the standard deviation for a measured distance of 25 cm is outside the sensors accuracy of ± 0.3 cm, showed in Table A.1. This might be due to not enough outliers are detected by the method in Section 3.2.4. A failure rate of 0.02 % might be too low in this case.

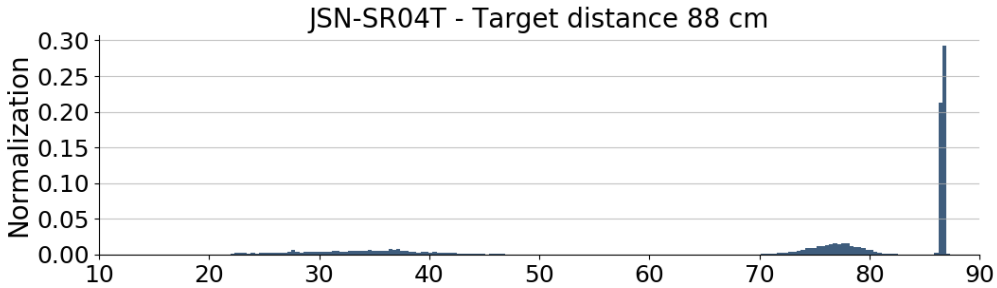

(a) A histogram over the experiment with 50 000 measurements of the sensor JSN-SR04T against a wall. The sensor was placed 88 cm away from the wall. The peak is located at 86.5 cm. There is a lot of noise, especially below the peak.

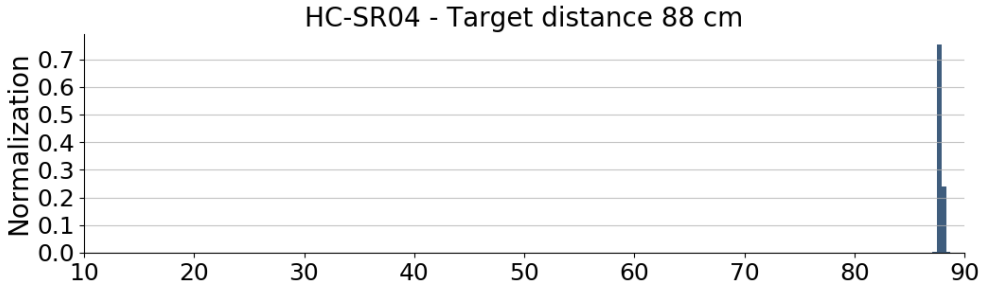

(b) A histogram over the experiment with 50 000 measurements of the sensor HC-SR04 against a wall. The sensor was place 88 cm away from the wall. The peak is located at 88 cm, where over 99 % of the measurements are located in a small vicinity of the peak.

Figure 4.1: A histogram from each sensor over the experiment with 50 000 measurements of the JSN-SR04T sensor and the HC-SR04 sensor against wall. Both sensors were placed 88 cm away from the wall and the experiment was conducted using one sensor at a time. The measured distance, the mean error, the standard deviation and the failure rate for the measurements are presented in Table 4.1.

The other standard deviation for a measured distance of 5 cm, 50 cm and 88 cm are more reasonable and in line with the datasheet for the HC-SR04 sensor, presented in Table 3.1. The standard deviation for a measured distance of 5 cm is higher than the other ones due to that the distance is close to the HC-SR04 sensors minimum range at 2 cm, presented in Table 3.1, resulting in a higher failure rate as well.

A failure rate of 0.75 % for the HC-SR04 sensor at a distance of 50 cm might also be a disputable result. Without that result the failure rate for the JSN-SR04T sensor is higher than that for the HC-SR04 sensor, indicating that the JSN-SR04T sensor receives more errors on longer distances. The maximum distance for the HC-SR04 sensor is larger than the maximum distance for the JSN-SR04T sensor presented in Equation 4.3 and Equation 4.5. This might be the reason that the HC-SR04 sensor has a lower failure rate at longer distances than the JSN-SR04T sensor. The JSN-SR04T sensor detects more objects than the target object. The standard deviation for the JSN-SR04T sensor is in line with the datasheets for the sensors presented in Table 3.1 with an accuracy for the JSN-SR04T sensor at ± 1 cm and for the HC-SR04 sensor at ± 0.3 cm.

Sensor	Measured distance [cm]	Mean error [cm]	Standard deviation [cm]	Failure rate [%]
JSN-SR04T	43	-0.96	0.09	0.20
HC-SR04	43	6.01	0.61	0.38

Table 4.2: The measured distance, the mean error, the standard deviation and the failure rate for the sensors for the second sensor experiment, with a drinking glass as the target object. At 43 cm the detected object was a round glass with a diameter of 8.5 cm standing in front of a wall at a distance of 88 cm away from the sensor. Only the largest peak is used in the table. The failure rate is all measurements that are not within the standard deviation, $2\,\sigma$, of the mean distance over the total number of measurements.

4.1.2 Sensor Experiment 2

The second sensor experiment, with a drinking glass as a target object, leading to the results in Table 4.2. Figure 4.2b and Figure 4.2a illustrate measurements against a drinking glass at a distance of 43 cm for the JSN-SR04T sensor and the HC-SR04 sensor, respectively. The JSN-SR04T sensor does not have much viable noise, only one large peak. This means that the sensor detects the drinking glass and reflects the waves. This proves that the JSN-SR04T sensor is therefore more precise in its measurements than the HC-SR04 sensor, explained in the previous paragraph and can be seen in Table 4.2. Figure 4.2b shows a smaller peak at around 94 cm indicating that the sensor gets reflections from both the drinking glass and the wall behind.

The mean errors are -0.96 cm for the JSN-SR04T sensor and 6.01 cm for the HC-SR04 sensor. This provides the information that around 1 cm needs to be removed from the results measured by the JSN-SR04T sensor when measuring on a drinking glass as the target object. The results in mean error differ from the mean error from Table 4.1 with around 1 cm, indicating that the JSN-SR04T sensor has difficulties detecting the drinking glass. However, the HC-SR04 sensor has more difficulties detecting the drinking glass, where the negative value for the HC-SR04 sensor is due to sensor failure and indicates that the distance between the sensor and the target object is further away than the actual mean error value.

The standard deviation is 0.10 cm for the JSN-SR04T sensor and 0.61 cm for the HC-SR04 sensor. The JSN-SR04T sensor is therefore more precise in its measurements than the HC-SR04 sensor. This precision might be due to the FoV for each sensor, 15° for the HC-SR04 sensor and 75° for the JSN-SR04T sensor.

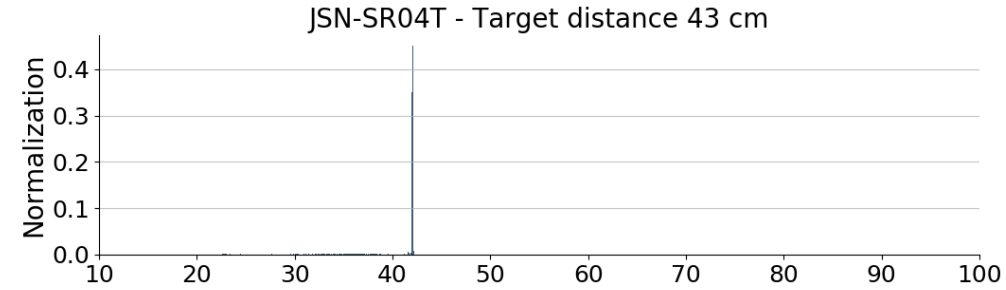

(a) A histogram over the experiment with 20 000 measurements of the sensor JSN-SR04T against a glass. The sensor was placed 43 cm away from the glass. The peak is located at 42.1 cm. There is noise in the lower parts of the histogram.

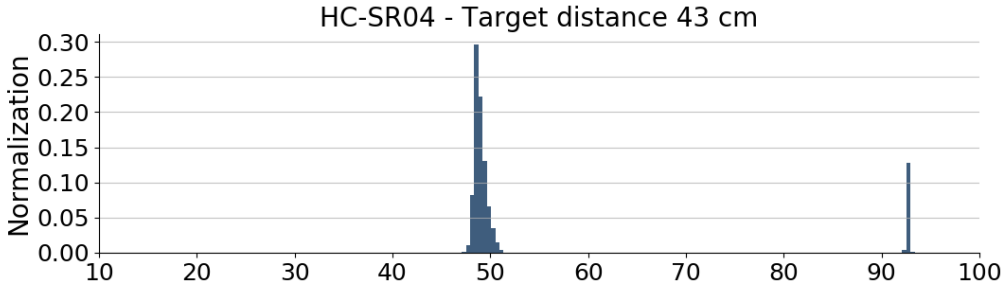

(b) The figure shows a histogram over the Ansor HC-SR04 against a glass of water. The sensor was placed 43 cm away from the glass. The right, smaller peak indicates detections from the wall behind the glass.

Figure 4.2: A histogram from each sensor over the experiment with 20 000 measurements of the JSN-SR04T sensor and the HC-SR04 sensor against a drinking glass with a diameter of 8.5 cm. The sensors was placed 43 cm from the drinking glass and the experiment was conducted using one sensor at the time. The measured distance, the mean error, the standard deviation and the failure rate for the measurements are presented in Table 4.2.

The standard deviation for the HC-SR04 sensor is outside the accuracy range provided by the datasheet presented in Table 3.1. The failure rate is slightly lower for the JSN-SR04T sensor than for the HC-SR04 sensor indicating that the JSN-SR04T sensor receives fewer errors on shorter distances than on larger distances and that the JSN-SR04T sensor is better at detecting the target object and not the wall behind the target object.

4.1.3 Comparison Between the HC-SR04 Sensor and the JSN-SR04T Sensor in the Sensor Experiment

There was a discrepancy between the measured distance and the distance detected by the sensor, presented in Table 4.2 and Table 4.1. For the JSN-SR04T sensor there is a multiplicative error for the mean value of the sensor. This error can have different causes. The JSN-SR04T sensor has a larger FoV at 75° [38] compared to the FoV for the HC-SR04 sensor at 15° [37]. As a result of the larger FoV for the JSN-SR04T sensor it might measure other points than the object that was meant to be measured. It can, therefore, be more difficult to categorise the measurements.

As presented in Table 4.1, the failure rate for the JSN-SR04T sensor is higher for larger distances (88 cm) than for shorter distances (43 cm). A failure rate that is almost twice the size for larger distances might cause problems since false detections can cause system failures and in turn accidents if used for example in an automated vehicle.

The HC-SR04 sensor has a very low failure rate when measuring against a flat wall, illustrated in Figure 4.1b. This might also be due to the smaller FoV for the HC-SR04 sensor. The FoV at 15° makes it easier to aim and only get the desired target object in the measurements. If the target object is smaller than the size of the preferred target object for the sensor at a certain distance, for example during the drinking glass experiment illustrated in Figure 4.2b, an failure occurs. The HC-SR04 sensor does in this case detect the target object but also the surrounding environment. This is shown by a peak at 88 cm representing the wall behind the drinking glass.

When measuring at the drinking glass with the JSN-SR04T sensor, it did not detect the wall behind the drinking glass. The positive value in Table 4.2 is due to sensor failure where the sensor indicates that the distance between the sensor and the target object is further away than the actual value. This might be due to that the HC-SR04 sensor has a smaller FoV than the JSN-SR04T sensor. The JSN-SR04T sensor seems to be better at detecting objects than the HC-SR04 sensor, but it might therefore also detect objects that are not of interest.

4.1.4 Introduction of the Generic Sensor Failure Model

The generic sensor failure model is a model to explain when an object no longer can be detected by the sensor. A threshold for the minimum signal is used to compute the maximum range that an object can be detected on.

$$\begin{aligned} S_{\text{min, sensor}} &= \frac{P_t G \sigma A_e}{(4\pi)^2 \cdot R_{\text{max}}^4} \\ &= \frac{\Omega}{(4\pi)^2 \cdot R_{\text{max}}^2} \cdot P_t G A_e \\ &= \frac{\text{FoV} \cdot \pi/180}{(4\pi)^2 \cdot 4^2} \cdot P_t G A_e \end{aligned} \tag{4.1}$$

$$S_{\text{min,HC-SR04}} = 1.03 \times 10^{-4}\,\text{m}^{-2} \cdot P_t G A_e \tag{4.2}$$

$$R_{\text{max,HC-SR04, object detection}} = \left[\frac{\sigma}{(4\pi)^2 \cdot 1.03 \times 10^{-4}\,\text{m}^{-2}} \right]^{1/4} \tag{4.3}$$

Equation 4.2 presents a lower bound for the HC-SR04 sensor, which has an maximum FoV of 15°. If the signal is smaller than the result of Equation 4.2, then the sensor will not be able to detect the object and it causes a sensor failure. The lower bound is usually the important bound since the measured object is not a perfectly flat wall. With the quantization noise found in the sensor, the target signal may become too low. There are three parameters (P_t, G, A_e) where the information can not be obtained in this project. This is however not a problem, since substituting Equation 4.2 into Equation 3.8 results in Equation 4.3.

In one of the measurements, illustrated in Figure 4.2b, a glass with cross-section $0.0105\,\text{m}^2$ was the target. This results in a maximum range for detecting the object at 0.90 m. By solving Equation 4.3 for σ, the measured cross-section would be $5.56 \times 10^{-4}\,\text{m}^2$. This is about half the size of the real cross-section for the target. This would indicate that the cross-section viewed by the sensor is only measured by the cross-section at 45° of the target.

$$S_{\text{min,JSN-SR04T}} = 2.30 \times 10^{-4}\,\text{m}^{-2} \cdot P_t G A_e \tag{4.4}$$

$$R_{\text{max,JSN-SR04T, object detection}} = \left[\frac{\sigma}{(4\pi)^2 \cdot 2.30 \times 10^{-4}\,\text{m}^{-2}} \right]^{1/4} \tag{4.5}$$

Equation 4.4 presents a lower bound for the JSN-SR04T sensor, which has an maximum FoV of 75°. As mentioned before, this is important since it should affect when

Sensor	Measured distance [cm]	Mean error [cm]	Standard deviation [cm]	Failure rate [%]
JSN-SR04T$_1$	86.8	3.35	0.41	0.43 %
HC-SR04$_1$	86.8	1.53	0.45	0.64 %
JSN-SR04T$_2$	89.2	3.95	0.38	0.31 %
HC-SR04$_2$	89.2	0.34	0.33	0.56 %

Table 4.3: The measured distance for the sensors HC-SR04 and JSN-SR04T when they are measuring at the same time during stand-still experiments. The failure rate is the measurements that are not within two standard deviations of the normal distribution over all measurements. The subscript 1 indicates using a wall with a 1.5 cm × 1 cm spline at the bottom and the subscript 2 indicates using a flat wall.

the sensor is able to detect an object. Comparing Equation 4.2 with Equation 4.4, the denominator in Equation 4.4 is larger, which indicates that JSN-SR04T may be worse than HC-SR04 at detecting objects.

$$R_{\text{max,HC-SR04}} = \left[\frac{\sigma_0 \cdot K_b}{(4\pi)^2 \cdot 1.03 \times 10^{-4}}\right]^{1/4} \tag{4.6}$$

By rewriting Equation 4.2 with a calibration factor, Equation 4.6 is gained. For the experiment with the glass, this calibration factor is 0.5. The calibration factor will depend on the density of the material which is measured and the roughness on the surface on the object.

4.2 Testing the Generic Sensor Failure Model Through Vehicle Experiments

The last part of the project was to test the generic sensor failure model on an automated vehicle. This was conducted using both JSN-SR04T and HC-SR04 sensors together against the wall in two experiments. In vehicle experiment 1 the vehicle started from the wall and drove back to a position of around 80 cm from the target and in vehicle experiment 2 the vehicle started from the wall, drove back to a position of around 150 cm and then drove forward to a position of around 50 cm from the target. Figure 3.5 shows the vehicle experiment 1 and Figure 3.6 shows the vehicle experiment 2. The measurement series were run for at least 20 000 measurements. A numerical solver that fits the peak of a normal distribution was used in both vehicle experiments. The results for vehicle experiment 1 are presented in Table 4.3 and the results for the vehicle experiment 2 are presented in Table 4.4. The headers in the tables are the same as in the sensor experiments in Section 4.1.1.

4.2.1 Vehicle Experiment 1

The first vehicle experiment, where the vehicle started from the wall and drove back to a position of around 80 cm from the target, leading to the results in Table 4.3. The mean error differs from 3.35 cm to 3.95 cm for the JSN-SR04T sensor and from 1.53 cm to 0.34 cm for the HC-SR04 sensor. This means that the JSN-SR04T sensor has a bias of 3 cm to 4 cm and that the HC-SR04 sensor has a bias of around 0.5 cm to 1.5 cm. This bias needs to be removed from the measured data to get a correct result. In the sensor experiments in Table 4.1, the mean error was different from the mean errors was smaller, which is due different reference points on the vehicle. Since the sensor was not placed at the same position as the front wheels, these measurements differ. But by comparing the different ranges and the relation between the two different sensors, one notice that the result is consistent with previous measurements.

The maximum detection distance for the HC-SR04 sensor is larger than the maximum distance for the JSN-SR04T sensor. There is a spline of one of the walls in Table 4.3 and the large differences in mean errors might be due too this spline. The HC-SR04 sensor might detect the spline but the JSN-SR04T sensor does not detect the spline, which in turn would indicate that the cross-section of the spline is too small for the JSN-SR04T sensor. However, the larger mean error in the results from the JSN-SR04T sensor for the flat wall indicates uncertainty in the results from the vehicle experiments. With the uncertainties of what could be detected the focus in the experiments was shifted from detecting smaller target objects to to begin with only detecting the wall.

The standard deviation differs from 0.38 cm to 0.41 cm for the JSN-SR04T sensor and 0.33 cm to 0.45 cm for the HC-SR04 sensor. These standard deviations are in line with the datasheets for the sensors presented in Table 3.1 with an accuracy for the JSN-SR04T sensor at ± 1 cm and for the HC-SR04 sensor at ± 0.3 cm. The failure rates in the vehicle stand-still experiment, where both sensors were used at the same time, are overall higher than those in the sensor experiment, where each sensor was used, respectively. The highest value for the HC-SR04 sensor is 0.28 cm for the sensor experiment and 0.64 cm for the vehicle experiment. The highest value for the JSN-SR04T sensor is 0.35 cm for the sensor experiment and 0.43 cm for the vehicle experiment. The failure rate is slightly lower for the JSN-SR04T sensor than that for the HC-SR04 sensor, indicating that the JSN-SR04T sensor slightly benefits from using both sensors at the same time but the HC-SR04 sensor does not.

Sensor	Target distance [cm]	Measured distance [cm]	Standard deviation [cm]	Failure rate [%]
HC-SR04	50	49.84	3.67	0.72 %
	150	152.21	4.10	0.72 %
JSN-SR04T	50	49.45	3.70	8.68 %
	150	151.86	6.49	8.68 %
HTC VIVE	50	47.67	3.56	0.56 %
	150	151.19	4.94	0.56 %

Table 4.4: The measured distance for the sensors HC-SR04 and JSN-SR04T when they are measuring at the same time during motion experiments. The failure rate is all measurements that are not within the standard deviation of the normal distribution. The measurements are taken against a white flat wall. Measured distance from previous tables is measured through the reference HTC VIVE system, since the system is automated.

4.2.2 Vehicle Experiment 2

The second vehicle experiment, with a wall as the target object where the vehicle started from the wall, drove back to a position of around 150 cm and then forward to a position around 50 cm from the target, leading to the result in Table 4.4. The results from the second vehicle experiment are shown in Figure 4.3. Most of the outliers for both sensors have been removed in the figures.

By removing outliers, a failure rate of 0.7 % for the HC-SR04 sensor and 8.7 % for the JSN-SR04T sensor was obtained. The outliers for the JSN-SR04T sensor are larger in the vehicle experiments than during the sensor experiments. One of the possible reasons why this happens is that the JSN-SR04T sensor has a larger FoV, described in Section 4.1.3. Figure 4.3c illustrates how precise the HTC VIVE system is during the second vehicle experiment, with a failure rate at 0.56 %. The mean error is not possible to achieve, during the second vehicle experiment, since the vehicle is automated during this experiment and the distances are not measured by a ruler.

The results from the second vehicle experiment in Figure 4.4 have larger standard deviations than the deviation for the first vehicle experiment, shown in Table 4.3. The standard deviation is a factor of ten larger for the second vehicle experiment. There are a couple of different factors that made measurements for the vehicle experiment much larger, for example, time delay for TCP (see Section 4.2.4) and the frequency of sensor measurements. The sampling speed for the sensors was between 7 Hz and 10 Hz which could result in the vehicle driving up to 20 cm between two measuring points. This could make the vehicle stop over 10 cm to late. Instead of only using the measurements that the sensors provided, an interpolation between the measurements was used. The speed between the two last measurements was computed.

Sensor	Target distance [cm]	Probability of crash [%]
HC-SR04	50	9.84 %
HC-SR04	150	27.58 %
JSN-SR04T	50	18.18 %
JSN-SR04T	150	33.45 %

Table 4.5: The probabilities of crash depending on the sensor and which distance it stopped at. The HC-SR04 sensor has a lower probability of crash than the JSN-SR04T sensor.

By measuring the time difference between the last measurement and the current time, an approximation of the position could be obtained. These improvements to the system caused it to be closer to the target distance. The standard deviations for both the HC-SR04 sensor and the JSN-SR04T sensor are out of the accuracy range presented in Table 3.1. An interesting aspect is that both sensors have similar standard deviations (around 3.7 cm) at the shorter distance of 50 cm, but the JSN-SR04T sensor has a standard deviation of 6.49 cm at a distance of 150 cm, while the HC-SR04 sensor has 4.1 cm. The JSN-SR04T sensor also has a significantly higher failure rate at 8.68 %, while the HC-SR04 sensor has 0.72 %. The HC-SR04 sensor is therefore more accurate during this vehicle experiment and has a failure rate closer to the failure rate of the reference HTC VIVE system.

4.2.3 The Probability of Crash

As a measurement of how good the emergency brake is working, the probability of crash is used. When measuring the probability of a crash, two different measurements are taken into account: the probability of detection and the probability of the wrong position. The probability of detection indicates how likely the sensor is able to detect the object. The probability of detection is calculated from the first vehicle experiment in Section 3.2.3.2. The equation for the probability of detection is shown in Equation 4.7. The failure rate for the sensors is the ratio between the measurements that are outside of two standard deviation for the sensor and all measurements.

$$P_{\text{crash}} = 1 - (1 - \text{failure rate sensor}) \cdot \text{probability of wrong position} \tag{4.7}$$

The probability of the wrong position is the cumulative probability that the vehicle is able to stop before a given threshold, which is shown in Figure 4.4. For the experiment, a threshold of 5 cm after the target distance was set. These are the red lines in Figure 4.4. The reason why 5 cm after the target distance was chosen, was due to the breaking distance of the vehicle. Table 4.5 presents the probabilities of crash for each of the two sensors, HC-SR04 and JSN-SR04T. The HC-SR04 sensor has a lower probability of crash than the JSN-SR04T sensor for both distances.

Mean value [ms]	Standard deviation [ms]	Min Value [ms]	Max Value [ms]	Packages lost [%]
12.58	41.24	1	445	0.1 %

Table 4.6: The delays received by sending messages through TCP. Large standard deviation indicates that the time delays are largely varying, which shows uncertainies in the delays.

4.2.4 Time Delay of TCP

When noticing the large distribution of stopping distances, one of the parameters that were reviewed was the time delay for the network. Table 4.6 is the result of running 10 000 measurements from a computer to the RPI3. The large standard deviation shows the unpredictability of the time delays. These results are of importance to the design of the system and with different design choices, the system could have been improved.

Since everything could not be implemented on the RPI3, a server-client model had to be implemented. This caused a delay between commands in the system between the server (RPI3) and the client (computer). This is presented in Table 4.6. The problem with the delay is that it is not constant in time. Depending on how much traffic the router has at a specific time, there is a different amount of lag. One improvement to the system would be to have a dedicated server that runs the experiments, but this was not possible to implement in the workplace. Another improvement for the vehicle experiments could be to have all the driving control on the RPI3. The reason for the system design used in this project was to be able to control the vehicle with the HTC VIVE system. This was later not implemented due to time constraints.

If the driving control of the vehicle was made from the RPI3, the unpredictable time delays for TCP would not exist and more precise brake distances could have been obtained. To be able to be more precise in the stops, the emergency brake could have been implemented on the server (RPI3) instead. This would prevent the delay which is a problem with a server-client model and could have improved the result. This was not implemented due to the time constraints of the project.

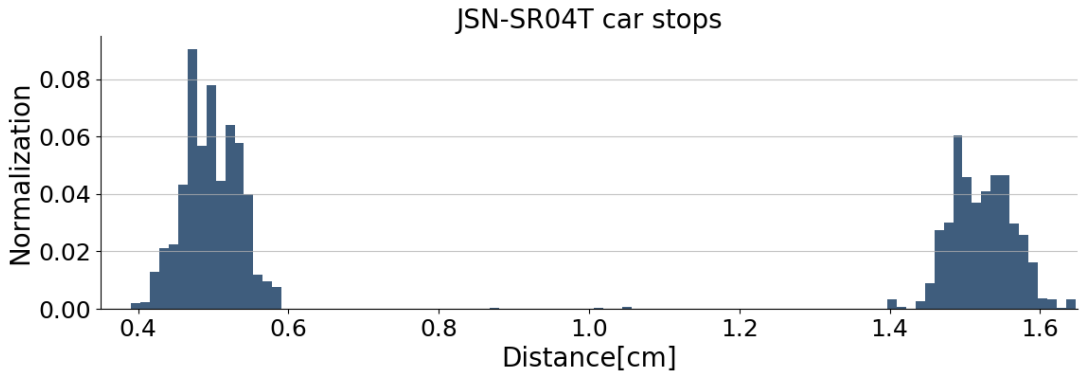

(a) The distributions of distances JSN-SR04T measured when the vehicle stopped at the target value. The target value for the shorter distance was 0.5 cm and the for the larger was 1.5 cm.

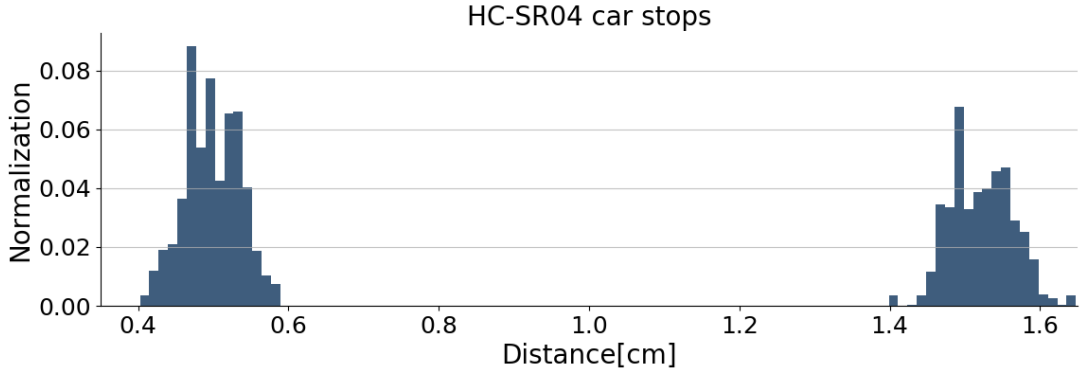

(b) The distributions of distances HC-SR04 measured when the vehicle stopped at the target value. The target value for the shorter distance was 0.5 cm and the for the larger was 1.5 cm.

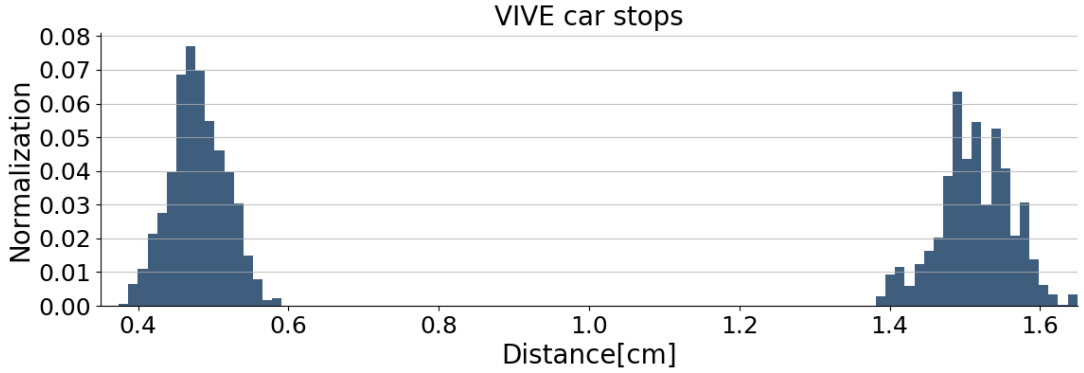

(c) The distributions of distances HTC VIVE measured when the vehicle stopped at the target value. The target value for the shorter distance was 0.5 cm and the for the larger was 1.5 cm.

Figure 4.3: The measurement series from the two sensors. Since both sensors are run at the same time, both figures should be the same, but due to different standard deviations the shapes become different.

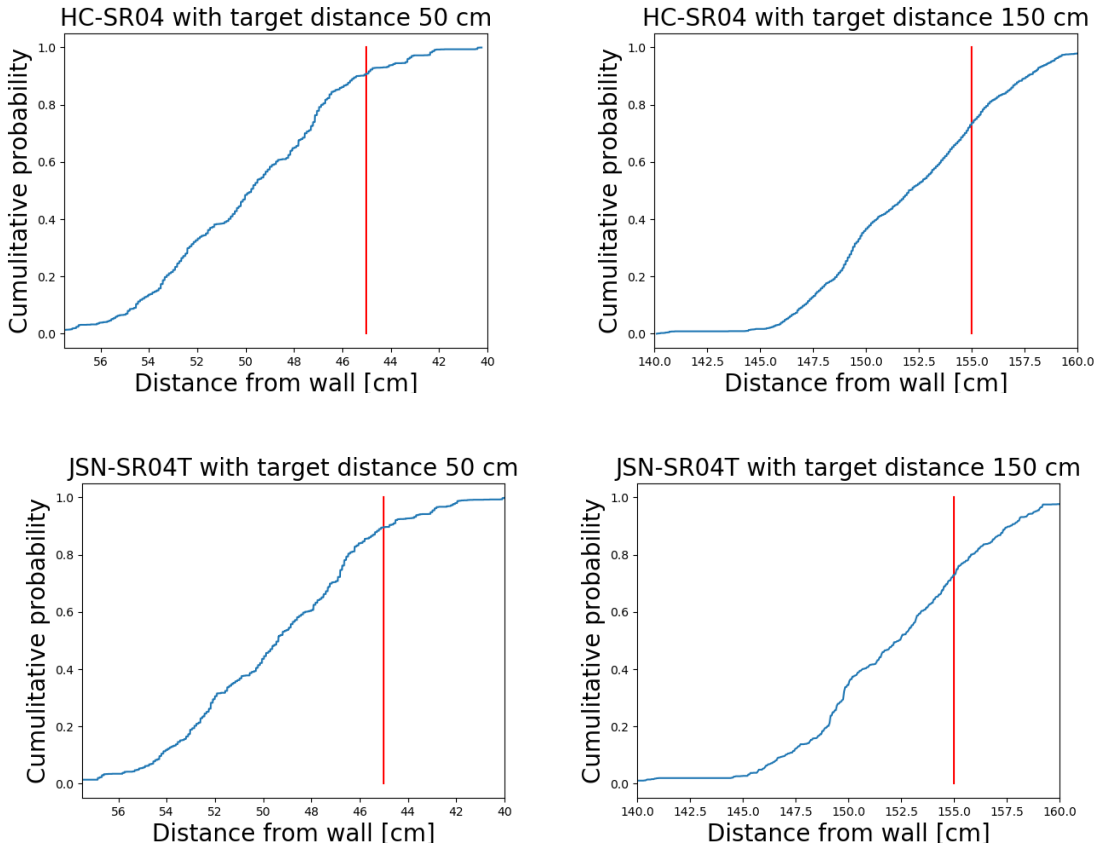

Figure 4.4: The cumulative probabilities for the sensors depend on the moving direction of the vehicle. The top figures shows the cumulative probabilities for the HC-SR04 sensor and the bottom two represent the cumulative probabilities for the JSN-SR04T sensor. The red lines are representing the threshold for when the vehicle has driven too far. For driving forward, the cumulative probability is higher for both sensors at the threshold. This indicates that the vehicle is more stable when driving forwards than backward.

5

Conclusions

The purpose of this thesis was to investigate if a generic failure model for ultrasonic sensors is able to predict how sensor failures affect a larger system. A failure model was deduced through the radar equations, with the purpose to determine when an object could be detected and not be detected by the ultrasonic sensors. This failure model was tested with a drinking glass as the target object to determine if it was feasible to detect the drinking glass or not. The generated failure model seemed to be able to determine the measurements of the object most of the time. However a calibration coefficient was needed due to the rounding appearance of the drinking glass.

When trying dynamic measurements with the vehicle, a couple of problems were discovered. One problem was that the vehicle was not able to drive in a straight line towards the target object. An attempt to modify the steering of the vehicle was performed, but a better result was not accomplished. The steering control problems made measurements with the vehicle against smaller target objects unattainable, since the smaller target object could not be in sight of the ultrasonic sensor throughout the entire measurement series.

Another situation with the dynamic vehicle measurement was the unstable time delay caused by the server-client model that were used. The time delay might have been mitigated in a couple of ways. Firstly, if the RPI3, instead of the computer, would have performed the calculations for the distance measurements of the ultrasonic sensors, the delay between a measurement and the vehicle taking an action could have been minimised. This could have decreased the probability of crash for the vehicle, since the reaction time for the system as a whole would be improved. The flaw with calculating the measurements on the computer instead of on the RPI3, was overlooked in the static sensor experiments, since the vehicle was standing still. Therefore the time delay was not noticed until during the dynamic part of the vehicle experiments (see further in Section 3.2.3.3). When the importance of the time delays were found, it was too late to change the system design.

During this study, a HTC VIVE system has been used as a general positioning system. During the first measurements with the HTC VIVE system, the difference between the measurements for the HTC VIVE system and reality was large. The differences may be due to the base stations in the systems were not well-positioned or that there was no real-world reference for the system. A study on how to minimize the wrong alignments in between the HTC VIVE system and real-life was found

[44]. They noticed in the study that there was a drift in the coordinate system for the HTC VIVE system. To solve the problems they were using three trackers as a reference system and were able to adjust their measurements to correlate for the drift.

What has been found in this study is that the uncertainty of the HTC VIVE system is good in a test environment, but can be unstable outside this environment. If considering a real environment, the deviations that were found might threaten the patient in an autonomous vehicle. If the environment consists of stairs and the HTC VIVE system is deviating too far from the real world, then it could cause an accident where the wheelchair is driving of the stairs. While safety measurements could be taken to avoid this, it could be dangerous with only the HTC VIVE system as a reference measurement.

There is also the matter of covering a whole room with the base stations and trackers. A study discusses how to cover a room with cameras with considerations of the costs [47]. The HTC VIVE system could be expensive used in a real-world environment since many trackers and base stations are needed. These optimizations are not in the scope of this report but show that there are more concepts to be considered before a HTC VIVE system can be considered a good positioning system. Using HTC VIVE as a positioning system for a medical autonomous vehicle, for example, an autonomous wheelchair, is not possible at the moment. Using ultrasonic sensors for detecting obstacles at medical autonomous vehicles is possible in experimental environment but more research in the area are necessary to ensure safety for the users in real life environment.

Bibliography

[1] M. Kyriakidis *et al.*, "Public opinion on automated driving: Results of an international questionnaire among 5000 respondents", *Transport Res F-Traf*, vol. 32, pp. 127–140, 2015.

[2] National Highway Traffic Safety Administration *et al.*, "Preliminary statement of policy concerning automated vehicles", *NHTSA*, p. 7, 2013.

[3] R. Benenson *et al.*, "Towards urban driverless vehicles", *IJVAS*, vol. 1/2, no. 6, pp. 4–23, 2008.

[4] D. Kramer *et al.*, "Regulation of medical devices in the united states and european union", *N Engl J Med*, vol. 366, no. 9, pp. 848–55, 2012.

[5] Swedish Institute for Standards, "Medical devices - application of risk management to medical devices (iso 14971:2019)", *Swedish Standard*, pp. 1–48, 2019.

[6] ——, "Medical device software - software life cycle processes", *Swedish standard*, pp. 1–170, 2019.

[7] L. Devigne *et al.*, "Design of an immersive simulator for assisted power wheelchair driving", *2017 ICORR*, pp. 995–1000, 2017.

[8] F. Routhier *et al.*, "Mobility and participation of people with disabilities using mobility assistive technologies: Protocol for a mixed-methods study", *JMIR*, vol. 8, no. 4, e12089, 2019.

[9] S. Bennett *et al.*, "Wheelchair accessibility: Descriptive survey of curb ramps in an urban area", *Disabil Rehabil*, vol. 4, no. 1, pp. 17–23, 2009.

[10] S. Stark *et al.*, "Development of a measure of receptivity of the physical environment", *Disabil Rehabil*, vol. 29, no. 2, pp. 123–137, 2007.

[11] S. Massengale *et al.*, "Effect of visual perception, visual function, cognition, and personality on power wheelchair use in adults", *Disabil Rehabil*, vol. 17, no. 2, pp. 108–121, 2005.

[12] D. M. Brienza and J. Angelo, "A force feedback joystick and control algorithm for wheelchair obstacle avoidance", *Disabil Rehabil*, vol. 18, no. 3, pp. 123–129, 1996.

[13] Department of Economic and Social Affairs, "Convention on the rights of persons with disabilities (uncrpd)", *European disability strategy 2010-2020*, 2010.

[14] United Nations, "Sustainable development goals", *SDG*, 2015.

[15] B. Paden *et al.*, "A survey of motion planning and control techniques for self-driving urban vehicles", *IEEE Intell Transp*, vol. 1, no. 1, pp. 33–55, 2016.

[16] P. Koopman and M. Wagner, "Challenges in autonomous vehicle testing and validation", *SAE J-Automot Eng*, vol. 4, no. 1, pp. 15–24, 2016.
[17] K. Kaur and G. Rampersad, "Trust in driverless cars: Investigating key factors influencing the adoption of driverless cars", *J Eng Technol Manage*, vol. 48, pp. 87–96, 2018.
[18] L. Hulse *et al.*, "Perceptions of autonomous vehicles: Relationships with road users, risk, gender and age", *Safety Sci*, vol. 102, pp. 1–13, 2018.
[19] S. Fioretti *et al.*, "A navigation system for increasing the autonomy and the security of powered wheelchairs", *IEEE T Rehabil Eng*, vol. 8, no. 4, pp. 490–498, 2000.
[20] G. Jäger *et al.*, "Generic sensor failure modeling for cooperative systems", *Sensors*, vol. 18, no. 3, p. 925, 2018.
[21] Automation Products group, *The difference between ultrasonic and radar level sensors*, 2019. [Online]. Available: `https://www.apgsensors.com/about-us/blog/radar-and-ultrasonic-sensors` (visited on 10/20/2019).
[22] L. Koval *et al.*, "Distance measuring by ultrasonic sensor", *IFAC Papersonline*, vol. 49, no. 25, pp. 153–158, 2016.
[23] G. Gibbs *et al.*, "Obstacle detection with ultrasonic sensors and signal analysis metrics", *Transp Res Proc*, vol. 28, pp. 173–182, 2017.
[24] M. Vellekoop, "Acoustic wave sensors and their technology", *Ultrasonics*, vol. 36, no. 1-5, pp. 7–14, 1998.
[25] K. Panda *et al.*, "Effects of environment on accuracy of ultrasonic sensor operates in millimetre range", *Perspect Sci*, vol. 8, pp. 574–576, 2016.
[26] K. Gillespie, *Ultrasonic sensors: Advantages and limitations*, 2017. [Online]. Available: `https://www.maxbotix.com/articles/advantages-limitations-ultrasonic-sensors.htm/` (visited on 09/14/2019).
[27] Fierce Electronics, *Long-range lidar sensor operates to 250 meters*, 2019. [Online]. Available: `https://www.fierceelectronics.com/sensors/long-range-lidar-sensor-operates-to-250-meters-0` (visited on 09/14/2019).
[28] W. Rees, *Physical Principles Of Remote Sensing*. Cambridge University Press, 2013.
[29] A. Castro, "Understand uncertainty for better test accuracy", *Microwaves RF*, vol. 52, no. 1, 2013.
[30] K. Jerath *et al.*, "Bridging the gap between sensor noise modeling and sensor characterization", *Measurement*, vol. 116, pp. 350–366, 2018.
[31] A. Birolini, *Reliability Engineering*. Springer, 2017.
[32] E. Ruijters and M. Stoelinga, "Fault tree analysis: A survey of the state-of-the-art in modeling, analysis and tools", *Computer Science Review*, vol. 15, pp. 29–62, 2015.
[33] R. Isermann, *Fault-Diagnosis Systems: An Introduction From Fault Detection To Fault Tolerance*. Springer Science & Business Media, 2006.
[34] J. Hovem, *Marine Acoustics: The Physics Of Sound In Underwater Environments*. Peninsula publishing Los Altos Hills, 2012.
[35] O. Sonbul and A. Kalashnikov, "Determining the operating distance of air ultrasound range finders: Calculations and experiments", *International Journal of Computing*, vol. 13, no. 2, pp. 125–131, 2014.

[36] Tutorialspoint, *Radar Systems - Range Equation*, 2020. [Online]. Available: `https://www.tutorialspoint.com/radar_systems/radar_systems_range_equation.htm` (visited on 10/06/2019).

[37] B. Bakker, *Ultrasonic Ranging Module HC - SR04*, 2020. [Online]. Available: `https://www.makerguides.com/hc-sr04-arduino-tutorial/` (visited on 09/14/2019).

[38] ——, *JSN-SR04T-2.0 datasheet*, 2020. [Online]. Available: `https://www.makerguides.com/jsn-sr04t-arduino-tutorial/` (visited on 09/14/2019).

[39] S. Yanbina *et al.*, "Design and simulation of the ultrasonic rangefinder based on micro-controller", *Physcs Proc*, vol. 25, pp. 1732–1737, 2012.

[40] T. Socolofsky and C. Kale, "A tcp/ip tutorial", *IETF*, 1991.

[41] R. Chen *et al.*, "Comparison of time to collision and enhanced time to collision at brake application during normal driving", *SAE Technical Paper*, 2016.

[42] D. Niehorster *et al.*, "The accuracy and precision of position and orientation tracking in the htc vive virtual reality system for scientific research", *i-Perception*, vol. 8, no. 3, p. 2 041 669 517 708 205, 2017.

[43] M. Borges *et al.*, "Htc vive: Analysis and accuracy improvement", in *2018 IROS*, IEEE, 2018, pp. 2610–2615.

[44] A. Peer *et al.*, "Vive tracking alignment and correction made easy", in *2018 VR*, IEEE, 2018, pp. 653–654.

[45] V. Chandola *et al.*, "Anomaly detection: A survey", *CSUR*, vol. 41, no. 3, pp. 1–58, 2009.

[46] W. Press and S. Teukolsky, "Savitzky-golay smoothing filters", *Comput Phys*, vol. 4, no. 6, pp. 669–672, 1990.

[47] U. Erdem and S. Sclaroff, "Optimal placement of cameras in floorplans to satisfy task requirements and cost constraints", 2004.

[48] Swedish Institute for Standards, *Electrically powered wheelchairs, scooters and their chargers - requirements and test methods*, 2009.

[49] ——, *Technical aids for disabled persons - environmental control systems for daily living (iso 16201:2006)*, 2006.

[50] ——, *Medical electrical equipment - part 1: General requirements for basic safety and essential performance*, 2006.

[51] ——, *Medical electrical equipment - part 1-4: General requirements for safety - collateral standard: Programmable electrical medical systems*, 2000.

[52] ——, *Medical electrical equipment - part 1-6: General requirements for basic safety and essential performance - collateral standard: Usability*, 2010.

[53] ——, *Medical electrical equipment - part 1-11: General requirements for basic safety and essential performance - collateral standard: Requirements for medical electrical equipment and medical electrical systems used in the home healthcare environment*, 2015.

[54] *Medical devices - part 1: Application of usability engineering to medical devices*, 2016.

A

Appendices

A.1 Sensor Information

	HC-SR04	JSN-SR04T
Operating Voltage	5 V	DC 3 V-5 V
Working Current	15 mA	Less than 8 mA
Probe Frequency	40 kHz	40 kHz
Max Range	4 m	6 m
Min Range	2 cm	20 cm
Distance accuracy	±3 cm	±1 cm
Measuring Angle	15°	75°
Trigger input signal	Input 10 µs high pulse	Input 10 µs high pulse
Echo Output Signal	Input TTL level signal and the range in proportion	Output pulse width level signal, or TTL
Dimension	L45xW20xH15 mm	L42xW29xH12 mm

Table A.1: Properties of the sensors collected from the datasheets [37, 38].

A.2 European Standards Regarding Medical Devices and Electrically Powered Wheelchairs

- EN 12184:2009 - Electrically powered wheelchairs, scooters and their chargers - Requirements and test methods [48].
- EN ISO 14971:2012 - Medical devices - Application of risk management to medical devices (ISO 14971:2007, Corrected version 2007-10-01) [5].
- EN ISO 16201:2006 - Technical aids for disabled persons - Environmental control systems for daily living (ISO 16201:2006) [49].
- EN 60601-1-1:2001 Medical electrical equipment - Part 1-1: General requirements for safety - Collateral standard: Safety requirements for medical electrical systems [50].
- EN 60601-1-4:1996 Medical electrical equipment - Part 1-4: General requirements for safety - Collateral standard: Programmable electrical medical systems [51].
- EN 60601-1-6:2010 Medical electrical equipment - Part 1-6: General requirements for basic safety and essential performance - Collateral standard: Usability [52].
- EN 60601-1-11:2010 Medical electrical equipment - Part 1-11: General requirements for basic safety and essential performance - Collateral standard: Requirements for medical electrical equipment and medical electrical systems used in the home healthcare environment [53].
- EN 62304:2006 Medical device software - Software life-cycle processes [6].
- EN 62366:2008 Medical devices - Application of usability engineering to medical devices [54].